Appl. Phys. A 57, 367–374 (1993)

Applied Physics A Solids and Surfaces

The Role of Excited Species in UV-Laser Materials Ablation

Part I: Photophysical Ablation of Organic Polymers

B. Luk'yanchuk[*], **N. Bityurin**[**], **S. Anisimov**[***], **D. Bäuerle**

Angewandte Physik, Johannes-Kepler-Universität Linz, A-4040 Linz, Austria (Fax: +43-732/2468-9242)

Received 11 May 1993/Accepted 2 June 1993

Abstract. UV-laser ablation is described in terms of a two-level system in which the excitation energy is dissipated via stimulated emission, thermal relaxation, and activated desorption of excited species. For thermal relaxation times $t_T > 10^{-9}$ s and $\Delta E^* \ll \Delta E$ (activation energies for excited-state and ground-state species) the model predicts high ablation rates at moderate surface temperatures, typically below 2000° C.

PACS: 82.65, 82.50, 42.10

Material removal caused by short high-intensity laser pulses is often denoted as pulsed-laser ablation. This process is of great relevance to numerous technological applications and it involves many fascinating aspects on the fundamentals of laser–solid interactions [1–3]. One of the basic questions in UV-laser ablation is concerned with the relative importance of thermal and non-thermal (photophysical or/and photochemical) mechanisms in the ablation process. This problem is extensively discussed in the literature, in particular with organic polymers where the UV-photon energy is comparable with the bond breaking energy [4–10]. Among the arguments frequently used in favor of a mainly photochemical process are:

(i) The observation that UV-laser-induced ablation of heat-sensitive materials such as organic polymers, can be performed almost without any damage of the remaining material, and in particular without indications for melting.

(ii) The non-equilibrium between the translational, vibrational, and rotational temperatures of ablated products.

(iii) The large number of species with high translational energies.

(iv) The differences in the composition of species obtained with UV- and IR-laser ablation.

(v) The very high temperatures that would be necessary to explain the experimentally observed ablation rates on the basis of a purely thermal model.

On the other hand, for a simple photochemical process, one would expect the ablated thickness to be dependent only on the total laser fluence (dose), and not on the laser-beam intensity and the dwell time separately, as found experimentally. An even more serious argument against a purely photochemical process, however, is the Arrhenius-type behavior of the ablation rate observed near the ablation threshold [9]. Last but not least it should be emphasized that the dominating ablation mechanism will depend on the particular material under investigation and the laser parameters employed.

The difficulty in the interpretation of the experimental results is closely related to the complexity of the optical excitation and energy-dissipation mechanisms involved in the ablation process. Let us consider this for the example of organic polymers [11]. In a simplified picture, UV radiation induces singlet–singlet transitions, for example $S_0 \rightarrow S_1$, as schematically shown in Fig. 1 (left-hand side). Under the action of intense laser light, the excited electron-vibrational

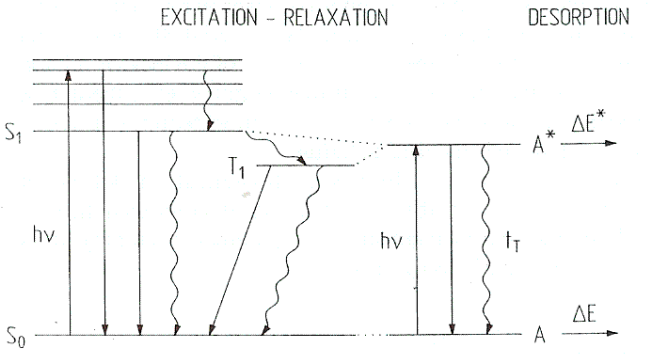

Fig. 1. Schematic showing electronic excitation and different energy relaxation channels for polymers (left). Here, we have drawn only the lowest excited singlet state S_1 and the triplet state T_1. The model employed in the paper is shown on the right-hand side of the figure. *Straight lines* indicate the absorption or emission of photons while *oscillating lines* indicate non-radiative processes

[*] On leave from General Physics Institute, Russian Academy of Sciences, 117942 Moscow, Russia

[**] On leave from Institute of Applied Physics, Russian Academy of Sciences, 603600 Nizhnii Novgorod, Russia

[***] On leave from L.D. Landau Theoretical Physics Intstitute, Russian Academy of Sciences, 142432 Chernogolovka, Moscow region, Russia

state may directly relax into the electronic ground state by stimulated emission of a photon. Alternatively, the system may first relax within the excited state S_1 (thermalization within the vibrational structure of S_1 occurs very fast, typically within $\leq 10^{-11}$ s). Subsequently, S_1 relaxes via transitions $S_1 \rightarrow S_0$ or via singlet-triplet interconversions $S_1 \rightarrow T_1$ and $T_1 \rightarrow S_0$. These transitions can take place via the emission of photons (fluorescence $S_1 \rightarrow S_0$ or phosphorescence $T_1 \rightarrow S_0$) or radiationless. The situation is similar for higher excited states S_2, T_2, etc.

The relative importance of different relaxation channels depends on the electronic structure of the chromophores. For example, for different chromophores the time of fluorescence varies, typically, between 10^{-11} s and 10^{-7} s [11]. The time for singlet-triplet interconversion depends on the energy difference between these states. If this energy difference is small as, for example, for the majority of aromatic ketons [11] and for some nitroaromatic compounds [12], singlet-triplet interconversion occurs within times of 10^{-12} s to 10^{-11} s and quantum efficiencies close to unity. The time for interconversion increases with increasing energy difference between the respective singlet and triplet states; it can vary significantly for transitions $S_1 \rightarrow T_1$, $S_2 \rightarrow T_2$, etc. The lifetime of triplet states is, typically, between 10^{-9} s and 10^{-4} s [11].

It is evident that the role of thermal and non-thermal mechanisms in pulsed-laser ablation is closely related to the different relaxation channels and the corresponding times involved. The situation is even more complicated. The laser-light intensities employed in pulsed-laser ablation yield high densities of excited species, induce multiple photon (non-linear) excitations, etc. This will not only result in changes of the characteristic relaxation times derived from experiments using UV-lamp irradiation but, additionally, will open up new relaxation channels. Clearly, these changes in excitation and energy-dissipation processes depend not only on the laser-beam intensity but on the duration of the laser pulse t_1 as well. In the total energy balance, we have to take into account excited species that leave the material surface before they transfer their excitation energy, or part of it, to the bulk. Non-radiative relaxation processes will result in a laser-induced temperature rise, the generation of internal stress, defects, etc. It is evident that all of these processes influence each other and depend on both the laser parameters and the physical properties of the particular material. Because of the complexity of the problem and because of the lack of reliable data on relaxation times, local temperatures. etc., theoretical models can only try to describe common features observed in laser-induced material ablation.

In this paper we discuss a theoretical model which describes UV-laser ablation in terms of combined thermal and non-thermal mechanisms. The parameters employed are typical for organic polymers.

1 Model

In the present model we assume that the total ablation velocity v is determined by both ground-state species A and electronically excited-state species A^*. The decomposition of species shall occur simultaneously with their desorption from the material surface. The excitation and energy relaxation process described by a two-level system where the transition $A \rightarrow A^*$ is induced by one-photon absorption. The respective number densities of species are N_A and N_{A^*}. The dissipation of the excitation energy $A^* \rightarrow A$ shall occur either via stimulated emission, or via non-radiative transitions. With the laser-light intensities under consideration, spontaneous emission can be ignored [13]. The non-radiative transitions shall be characterized by a single thermal relaxation time t_T, which shall be independent of temperature. Additionally, we assume that part of the total excitation energy is lost via activated desorption of excited species.

The laser beam shall propagate in z-direction; the ablated surface shall be placed within the plane $z = 0$. The radius of the laser beam w shall be large compared to the optical and thermal penetration depths which are denoted by l_α and l_T, respectively. With this condition, the problem can be treated in one dimension. The desorption rates related to species A and A^* depend on their respective activation energies ΔE and ΔE^*, and on the local temperature rise which is controlled by t_T. Thus, in the simplest case where we ignore any cooperative phenomena in the desorption process, the velocity v can be described by

$$v = k_A \mathscr{N}_\mathrm{S} + k_{A^*} \mathscr{N}_\mathrm{S}^* \tag{1}$$

where $k_A = v_A \exp[-\Delta E/T_\mathrm{S}]$ and $k_{A^*} = v_{A^*} \exp \times[-\Delta E^*/T_S]$ are the rate constants for activated desorption of ground-state and excited state species, respectively. $\mathscr{N} = N_A/N$ and $\mathscr{N}^* = N_{A^*}/N$ are the normalized densities of species where $N = N_A + N_{A^*}$ is the number density of chromophores which is, typically, $N = 6 \times 10^{21}$ cm^{-3} [8]. The index s refers to the surface, i.e. to $z = 0$. For the activation energies we assume $\Delta E^* \ll \Delta E$ and, additionally, that ΔE is of the order of the bond breaking energy. In the further calculations we set $\Delta E = 3$ eV and $\Delta E^* = 0.3$ eV. The velocities v_A and v_{A^*} are related to the attempt (vibrational) frequencies for non-excited and excited species, respectively. They are of the order of the sound velocity. We set $v_A = 3 \times 10^5$ cm/s and estimate $v_{A^*} \approx [\Delta E^*/\Delta E]^{1/2} v_A \approx 10^5$ cm/s.

In a coordinate system that is fixed to the substrate surface to be ablated, the density of species can be described by

$$\frac{\partial N_{A^*}}{\partial t} = v \frac{\partial N_{A^*}}{\partial z} + \frac{\sigma I}{h\nu}\left(N_A - N_{A^*}\right) - k_\mathrm{T} N_{A^*}\,, \tag{2}$$

$$\frac{\partial N_A}{\partial t} = v \frac{\partial N_A}{\partial z} - \frac{\sigma I}{h\nu}\left(N_A - N_{A^*}\right) + k_\mathrm{T} N_{A^*}\,, \tag{3}$$

where σ is the absorption cross section, I the laser-light intensity, and $k_\mathrm{T} = t_\mathrm{T}^{-1}$ the rate constant for thermalization of the excitation energy. Here, we ignore any diffusion processes which are slow compared to all other processes under consideration.

The propagation of the laser light within the substrate shall be described by

$$\partial I/\partial z = -\sigma(N_A - N_{A^*})I\,. \tag{4}$$

The heating of the solid surface is described by the heat-diffusion equation

$$\frac{\partial T}{\partial t} = v \frac{\partial T}{\partial z} + D_\mathrm{T} \frac{\partial^2 T}{\partial z^2} + \frac{D_\mathrm{T}}{\kappa} Q\,, \tag{5}$$

where κ is the thermal conductivity and D_T the thermal diffusivity. The heat source Q is determined by the non-radiative transitions and it is given by

$$Q = k_T h\nu N_{A^*} . \tag{6}$$

The heat flux at the surface $z = 0$ is dominated by the heat loss due to ablation. In accordance with (1), this is described by

$$\kappa \left.\frac{\partial T}{\partial z}\right|_{z=0} = \varrho\left(\Delta H\, k_A \mathcal{N}_S + \Delta H^*\, k_{A^*} \mathcal{N}_S^*\right) . \tag{7}$$

Here, we ignore possible differences in mass densities due to the excitation of species, i.e. we set $\varrho = \varrho^*$. This approximation does not hold for materials where stresses within the substrate surface which are caused, e.g., by laser-induced bond breaking, significantly influence the ablation rate [14]. For the transition enthalpies we set $\Delta H = \Delta E/M = 10^3$ J/g and $\Delta H^* = \Delta E^*/M = 10^2$ J/g, where M is the (average) mass of ablated fragments. Besides of (7), we employ the boundary conditions

$$\begin{aligned} &N_A(z \to \infty) = N , \qquad N_{A^*}(z \to \infty) = 0 , \\ &T(z \to \infty) = T(\infty) , \qquad I(z = 0) = I_S(t) , \end{aligned} \tag{8}$$

where $I_S(t)$ is the non-reflected part of the laser-light intensity on the substrate surface. Due to the attenuation of the incident laser-light intensity I_0, within the plasma plume, we have $I_S < I_0$. The initial conditions are

$$\begin{aligned} &N_A(t = 0) = N , \qquad N_{A^*}(t = 0) = 0 , \\ &T(t = 0) = T(\infty) . \end{aligned} \tag{9}$$

Equations (1–9) characterize the boundary-value problem. Any temperature dependences in material parameters are ignored. For the further calculations it is convenient to transform this problem to dimensionless variables which are denoted by the same letters in script, i.e.

$$\begin{aligned} &\mathcal{T} = T/T_0 , \quad \mathcal{T}(\infty) = T(\infty)/T_0 , \quad \Delta\mathcal{T} = \mathcal{T} - \mathcal{T}(\infty) , \\ &\mathcal{z} = z/z_0 , \\ &\mathcal{t} = t/t_0 , \quad \mathcal{t}_T = t_T/t_0 , \quad \mathcal{t}_1 = t_1/t_0 , \quad \mathcal{v} = v/v_0 , \\ &\mathcal{I} = I/I_b , \quad \mathcal{I}_S(t) = I_S(t)/I_b . \end{aligned}$$

Here, we use characteristic scaling values given by $T_0 = h\nu N D_T/\kappa$,

$$z_0^{-1} = \sigma N, \text{ and } t_0 = h\nu/I_b\sigma, \quad v_o = z_0/t_0 = I_b/h\nu N .$$

$I_b = 10^7$ W/cm^2 is of the order of the threshold intensity for ns-pulses. The other dimensionless parameters are:

$$\begin{aligned} &\mathcal{E} = \Delta E/T_0 , \quad \mathcal{E}^* = \Delta E^*/T_0 , \quad \mathcal{v}_A = v_A/v_0 , \\ &\mathcal{v}_{A^*} = v_{A^*}/v_0 , \\ &\zeta = \varrho v_A \Delta H/I_b , \quad \zeta^* = \varrho v_{A^*} \Delta H^*/I_b , \\ &\mathcal{D}_T = D_T/v_0 z_0 = D_T h\nu\sigma N^2/I_b . \end{aligned} \tag{10}$$

Values typical for UV-laser ablation of polymers are: $h\nu = 10^{-18}$ J ($\lambda = 200$ nm) and $\sigma = 10^{-17}$ cm^2 (strongly absorbing polymers) to 10^{-18} cm^2 (weakly absorbing polymers). The scaling factors are then

$$\begin{aligned} &T_0 = 4 \times 10^3 \text{ K} , \qquad z_0 = 1.7 \times (10^{-5}\text{–}10^{-4}) \text{ cm} , \\ &t_0 = 10^{-8}\text{–}10^{-7} \text{ s} , \quad v_0 = 1.7 \times 10^3 \text{ cm/s} . \end{aligned} \tag{11}$$

The dimensionless parameters become

$$\begin{aligned} &\mathcal{E} = 8.25 , \quad \mathcal{E}^* = 0.825 , \quad \mathcal{v}_A = 180 , \quad \mathcal{v}_{A^*} = 60 , \\ &\zeta = 30 , \quad \zeta^* = 1 , \quad \mathcal{D}_T = 3.6 \times (10^{-2} - 10^{-3}) , \\ &\mathcal{T}(\infty) = 7.5 \times 10^{-2} . \end{aligned} \tag{12}$$

For this parameter set we shall discuss the characteristics of ablation as a function of the intensity $\mathcal{I}_S$, the thermal relaxation time $\mathcal{t}_T$, and the absorption coefficient $\alpha = \sigma N$.

With the dimensionless variables the boundary-value problem can be written as:

$$\frac{\partial \mathcal{N}^*}{\partial \mathcal{t}} = \mathcal{v}\frac{\partial \mathcal{N}^*}{\partial \mathcal{z}} + \mathcal{T}(1 - 2\mathcal{N}^*) - \mathcal{k}_T \mathcal{N}^* , \tag{13}$$

$$\frac{\partial \mathcal{T}}{\partial \mathcal{z}} = -(1 - 2\mathcal{N}^*)\mathcal{T} , \tag{14}$$

$$\frac{\partial \mathcal{T}}{\partial \mathcal{t}} = \mathcal{v}\frac{\partial \mathcal{T}}{\partial \mathcal{z}} + \mathcal{D}_T \frac{\partial^2 \mathcal{T}}{\partial \mathcal{z}^2} + \mathcal{k}_T \mathcal{N}^* , \tag{15}$$

where $\mathcal{k}_T = 1/\mathcal{t}_T$. The velocity $\mathcal{v}$ can be determined from

$$\mathcal{v} = (1 - \mathcal{N}_S^*)\mathcal{v}_A \Pi(\mathcal{T}_S) + \mathcal{N}_S^* \mathcal{v}_{A^*} \Pi^*(\mathcal{T}_S) , \tag{16}$$

where $\Pi(\mathcal{T}_S) = \exp(-\mathcal{E}/\mathcal{T}_S)$ and $\Pi^*(\mathcal{T}_S) = \exp \times(-\mathcal{E}^*/\mathcal{T}_S)$. The boundary conditions are:

$$\begin{aligned} &\mathcal{D}_T \left.\frac{\partial \mathcal{T}}{\partial \mathcal{z}}\right|_{\mathcal{z}=0} = (1 - \mathcal{N}_S^*)\zeta\Pi(\mathcal{T}_S) + \mathcal{N}_S^* \zeta^* \Pi^*(\mathcal{T}_S) , \\ &\mathcal{N}^*(\mathcal{z} \to \infty) = 0 , \quad \Delta\mathcal{T}(\mathcal{z} \to \infty) = 0 , \\ &\mathcal{T}(\mathcal{z} = 0) = \mathcal{T}_S(\mathcal{t}) \end{aligned} \tag{17}$$

The initial conditions are:

$$\mathcal{N}^*(\mathcal{t} = 0) = 0 , \qquad \Delta\mathcal{T}(\mathcal{t} = 0) = 0 . \tag{18}$$

The total thickness of the ablated layer per pulse is

$$h_t = \int_0^\infty \bar{v}(t)\mathrm{d}t \approx h_1 + h_2 + h_3 ,$$

where $\bar{v} = v - v[T_S = T(\infty)]$, h_1 is the ablated layer thickness during the transition state $t < t_v$ before significant material ablation starts, $h_2 = v_S(t_1 - t_v)$ is the ablated thickness within the regime of stationary ablation $t_v \le t \le t_1$, h_3 refers to the time after the laser pulse $t > t_1$. Here, ablation may continue for a certain time due to the energy stored within the irradiated surface layer [5]. Clearly, with picosecond or femtosecond pulses the regime of stationary ablation may not be reached. With such short laser pulses, multiple-photon absorption processes become important.

2 Stationary Solutions

We now concentrate on stationary solutions of the boundary-value problem. Stationary solutions are of particular importance in nonlinear problems because they permit to deter-

mine the typical values of the various quantities. We consider a single laser pulse whose intensity on the ablated surface is constant, $I_S = \text{const}$. If we set all time derivatives in (13–15) equal to zero we obtain the first integral

$$\mathscr{D}_T \frac{\partial \tilde{\mathscr{T}}}{\partial x} = \tilde{\mathscr{T}} - \tilde{v}(\Delta\tilde{\mathscr{T}} + \tilde{\mathscr{N}}^*) . \tag{19}$$

The tilde indicates stationary quantities. From (19) and the boundary condition (17) we obtain

$$\tilde{v} = \frac{1}{\Delta\tilde{\mathscr{T}}_S + \tilde{\mathscr{N}}_S^*}\left[\mathscr{T}_S - (1-\tilde{\mathscr{N}}_S^*)\zeta\Pi(\tilde{\mathscr{T}}_S) - \tilde{\mathscr{N}}_S^*\zeta^*\Pi^*(\tilde{\mathscr{T}}_S)\right] . \tag{20}$$

From (20) and (16), we obtain the equation for the density of excited species at the surface

$$A\tilde{\mathscr{N}}_S^{*2} + B\tilde{\mathscr{N}}_S^* + C = 0 , \tag{21}$$

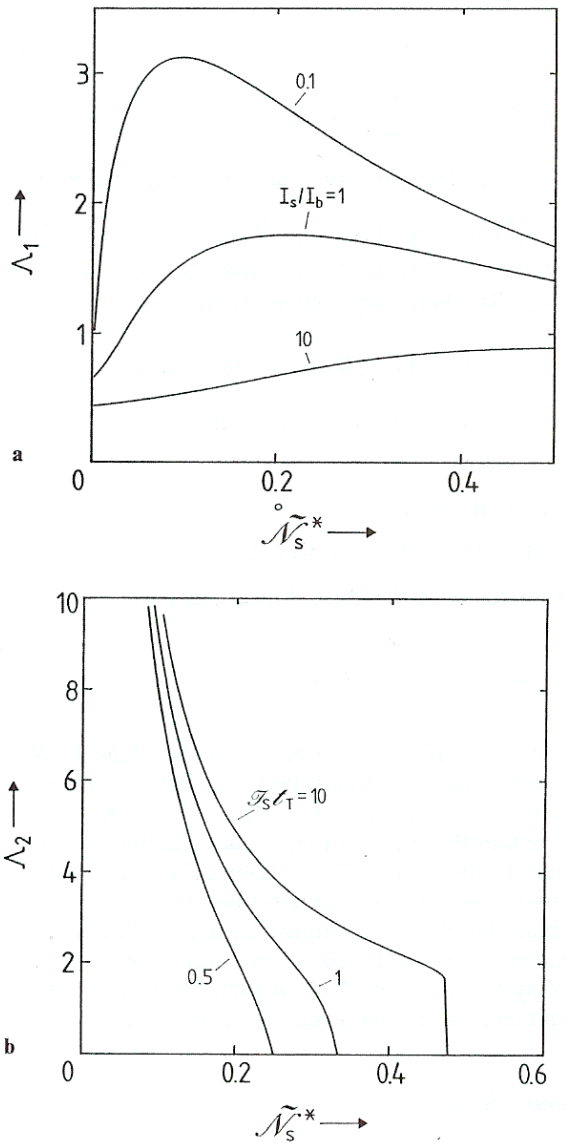

Fig. 2. a Dependence of the functions Λ_1 and Λ_2 [see (22) and (25)] on $\tilde{\mathscr{N}}_S^*$ for different values of $\mathscr{T}_S \equiv I_S/I_b$ and **b** for different values of $\mathscr{T}_S\ell_T$

where

$$A = A(\tilde{\mathscr{T}}_S) = \tilde{v}_A\Pi(\tilde{\mathscr{T}}_S) - v_{A^*}\Pi^*(\tilde{\mathscr{T}}_S) ,$$
$$B = B(\tilde{\mathscr{T}}_S) = A\Delta\tilde{\mathscr{T}}_S + (\zeta - \tilde{v}_A)\Pi(\tilde{\mathscr{T}}_S) - \zeta^*\Pi^*(\tilde{\mathscr{T}}_S) ,$$
$$C = C(\tilde{\mathscr{T}}_S) = \mathscr{T}_0 - (\zeta + \tilde{v}_A\Delta\tilde{\mathscr{T}}_S)\Pi(\tilde{\mathscr{T}}_S) .$$

From (20) and (21) we obtain the equation

$$\tilde{v} = \mathscr{T}_S\Lambda_1(\mathscr{T}_S, \tilde{\mathscr{N}}_S^*) . \tag{22}$$

The function Λ_1 is shown in Fig. 2a for different values of $\mathscr{T}_S \equiv I_S/I_b$. Here, the parameters given in (12) have been employed.

With $t_T = \text{const}$. (13) and (14) become independent from (15) and they can be written as

$$\frac{d\tilde{\mathscr{N}}^*}{d\eta} = \frac{\mathscr{T}_S}{\tilde{v}}\left(1 - \frac{1}{\mathscr{T}_S\ell_T}\frac{\tilde{\mathscr{N}}^*}{\eta(1-2\tilde{\mathscr{N}}^*)}\right) \tag{23}$$

with $\eta = \tilde{\mathscr{T}}/\mathscr{T}_S$ and the boundary conditions

$$\tilde{\mathscr{N}}^*(\eta = 1) = \tilde{\mathscr{N}}_S^* \quad \text{and} \quad \tilde{\mathscr{N}}^*(\eta = 0) = 0 . \tag{24}$$

Integration of (23) from $\eta = 0$ to $\eta = 1$ permits to calculate the Eigenvalues $\tilde{v}(\tilde{\mathscr{N}}_S^*)$. The asymptotic value of the right part of (23) for $\eta = 0$ is

$$\left.\frac{d\tilde{\mathscr{N}}^*}{d\eta}\right|_{\eta=0} = \frac{\mathscr{T}_S\ell_T}{1 + \tilde{v}\ell_T} .$$

The accuracy of the integration can be tested from

$$\tilde{v} = \frac{\mathscr{T}_S}{\tilde{\mathscr{N}}_S^*}\left[1 - \frac{1}{\mathscr{T}_S\ell_T}\int_0^\infty \tilde{\mathscr{N}}^*(x)\,dx\right] .$$

From (23) and (24) we obtain the additional equation

$$\tilde{v} = \mathscr{T}_s\Lambda_2(\mathscr{T}_s t_T, \tilde{\mathscr{N}}_s^*) . \tag{25}$$

Thus, in order to find $\tilde{v}$ and $\tilde{\mathscr{N}}_S^*$ we have to solve the system of transcendental equations (22) and (25). For the case $\mathscr{T}_S\ell_T \ll 1$ we can solve (23) analytically, giving

$$\Lambda_2 \approx \frac{1}{\tilde{\mathscr{N}}_S^*} - \frac{1}{\mathscr{T}_S\ell_T} . \tag{26}$$

On the other hand, if $\mathscr{T}_S\ell_T \gg 1$ and $\mathscr{N}_0 - \tilde{\mathscr{N}}_S^* \ll \mathscr{N}_0$ where $\mathscr{N}_0 \equiv \mathscr{N}_S^*(\tilde{v} = 0)$ we obtain

$$\Lambda_2 \approx 1/\tilde{\mathscr{N}}_S^* . \tag{27}$$

Figure 2b shows $\Lambda_2 = \tilde{v}/\mathscr{T}_S$ as a function of $\tilde{\mathscr{N}}_S^*$ for different values of $\mathscr{T}_S\ell_T$.

The spatial distribution of $\tilde{\mathscr{T}}(x)$ and $\tilde{\mathscr{N}}^*(x)$ for the limiting case $\tilde{v} = 0$ can directly be derived from (13) and (14) which yields

$$2\mathscr{T}_S\ell_T(1 - \tilde{\mathscr{T}}/\mathscr{T}_S) + \ln(\mathscr{T}_S/\tilde{\mathscr{T}}) = x \tag{28}$$

and

$$\tilde{\mathscr{N}}^*(x) = \tilde{\mathscr{T}}(x)\ell_T/[1 + 2\tilde{\mathscr{T}}(x)\ell_T] . \tag{29}$$

The limiting value $\mathcal{N}_0$ is given by

$$\mathcal{N}_0 = \mathcal{I}_S \varkappa_T / (1 + 2\mathcal{I}_S \varkappa_T) . \quad (30)$$

The density of excited species $\tilde{\mathcal{N}}_S$ can be calculated from the equation

$$A_1(\mathcal{I}_S, \tilde{\mathcal{N}}_S^*) = A_2(\mathcal{I}_S \varkappa_T, \tilde{\mathcal{N}}_S^*) . \quad (31)$$

Together with (20) and (21) we can also calculate $\tilde{v}$ and $\Delta\tilde{\mathcal{T}}_S$.

3 Results and Discussion

We now discuss the results of the model calculations. First, we consider the stationary ablation velocity $\tilde{v}$, the surface temperature rise $\Delta\tilde{\mathcal{T}}_S$, and the surface concentration of excited species $\tilde{\mathcal{N}}_S^*$, as a function of the intensity $\mathcal{I}_S$. We then discuss the spatial distribution of $\Delta\tilde{\mathcal{T}}(x)$, $\tilde{\mathcal{N}}^*(x)$ and $\tilde{\mathcal{T}}(x)$.

Figure 3 shows the velocity $\tilde{v}$ as a function of $\mathcal{I}_S \equiv I_S/I_b$ for different relaxation times $\varkappa_T$. It becomes evident that $\tilde{v}$ increases with $\varkappa_T$. If we consider, for example, $\mathcal{I}_S = 2$ and $\varkappa_T = 0.01$ we obtain for strongly absorbing polymers $\tilde{v} = 2 \times 10^3$ cm/s. For 10 ns pulses these values correspond to a fluence of 200 mJ and an ablated layer thickness of 0.2 μm/pulse. This result is in reasonable agreement with experimental findings [4].

The dependence of the surface temperature rise $\Delta\tilde{\mathcal{T}}_S \equiv \Delta\tilde{T}_S/T_0$ on the intensity $\mathcal{I}_S \equiv I_s/I_b$ is plotted in Fig. 4 for different values of $\varkappa_T$. The full curves refer to the activation energy $\Delta E = 3$ eV. With intensities $\mathcal{I}_S = 1$–10 ($I_S = 10^7$–10^8 W/cm^2) and a thermal relaxation time $\varkappa_T = 0.01$ ($t_T \approx 10^{-10}$ s) ablation requires a surface temperature rise of $\Delta\tilde{\mathcal{T}} \approx 1.25$–$1.75$ ($T_S \approx 5$–$7 \times 10^{3\circ}$ C). With $\varkappa_T \geq 0.1$ the surface temperature near the ablation threshold is below $2 \times 10^{3\circ}$ C. This is in agreement with experimental data on

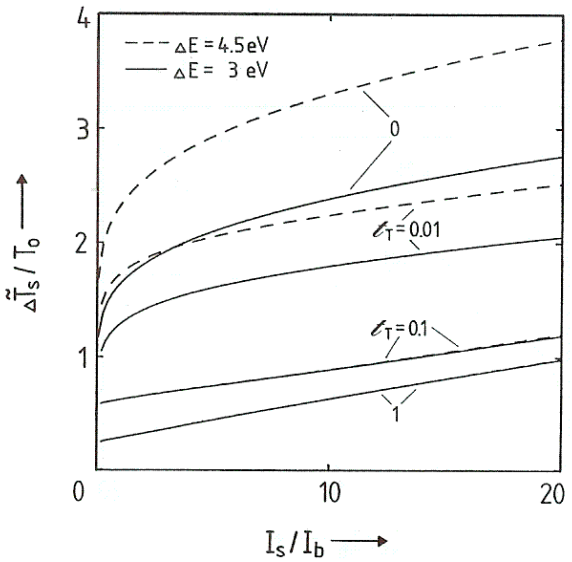

Fig. 4. Surface temperature rise $\Delta\tilde{\mathcal{T}}_S \equiv \Delta\tilde{T}_S/T_0$ as a function of the laser-light intensity $\mathcal{I}_S \equiv I_S/I_b$ for different relaxation times $\varkappa_T$. *Full* and *dashed curves* refer to activation energies $\Delta E = 3$ eV and 4.5 eV, respectively

the vibrational temperature of product species in polymer ablation [4]. With higher activation energies, the differences between thermal and photophysical ablation become even more pronounced. This can be seen from the dashed curves in Fig. 4, which have been calculated for $\Delta E = 4.5$ eV and otherwise unchanged parameters. For a purely thermal process, i.e. $\varkappa_T = 0$ and $I_S/I_b = 10$, the surface temperature rise $\Delta\tilde{T}_S/T_0$ increases by a factor of about 1.4. For times $\varkappa_T > 0.1$, however, the deviations between full and dashed curves can be ignored. The figure also shows that $\Delta\tilde{\mathcal{T}}_S$ decreases with increasing $\varkappa_T$. Thus, "cold" ablation which is related to the desorption of excited species becomes increasingly important. This is supported by the results shown in Fig. 5. The concentration of excited species $\tilde{\mathcal{N}}_S^*$,

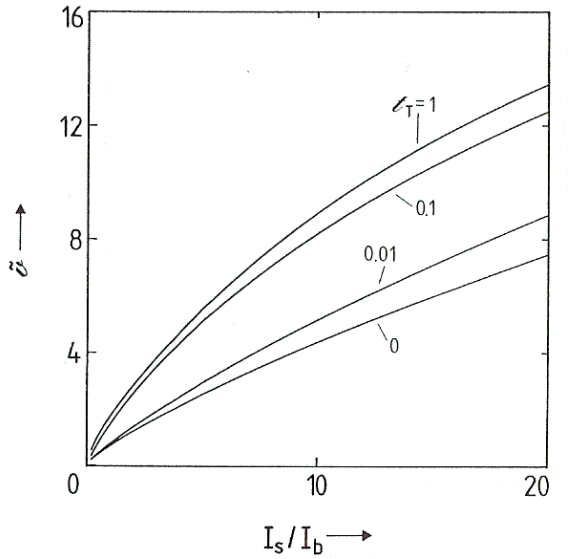

Fig. 3. Stationary ablation velocity $\tilde{v}$ as a function of $\mathcal{I}_S \equiv I_S/I_b$ for different relaxation times $\varkappa_T$

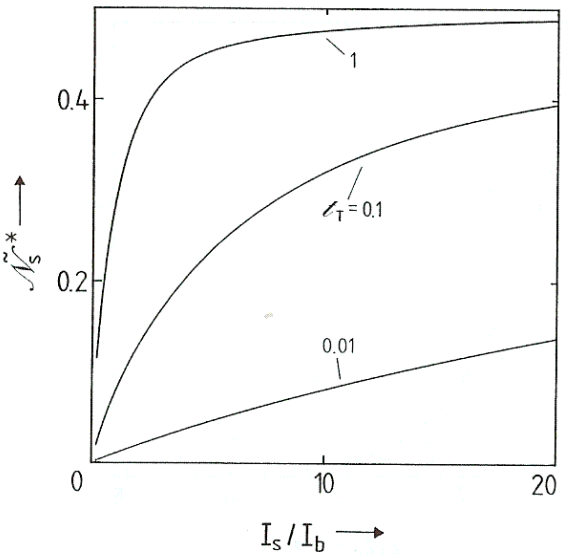

Fig. 5. Concentration of excited species on the surface, $\tilde{\mathcal{N}}_S^* \equiv \tilde{\mathcal{N}}^*(x = 0)$ as a function of intensity $\mathcal{I}_S \equiv I_S/I_b$ for different values of $\varkappa_T$

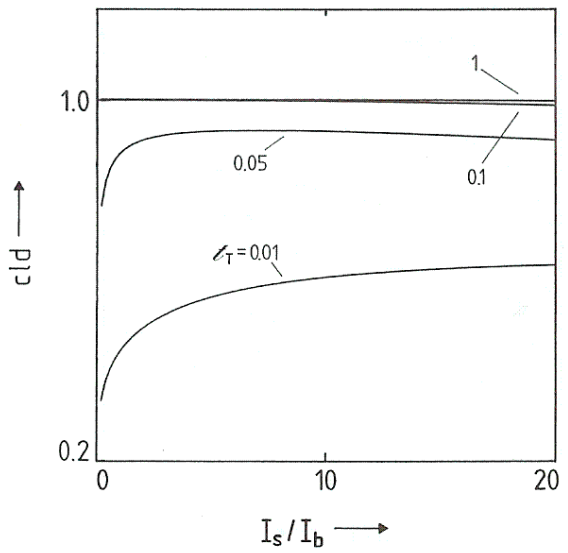

Fig. 6. Coldness cld [see (32)] as a function of $\mathcal{I}_S \equiv I_S/I_b$ for different values of $\mathcal{A}_T$

strongly increases with $\mathcal{A}_T$ and saturates for high intensities $\mathcal{I}_S \equiv I_S/I_b$.

To characterize the type of ablation mechanism, we define the coldness

$$\text{cld} = k_{A^*}\tilde{\mathcal{N}}_S^*/\tilde{v}\,. \tag{32}$$

The value cld $= 0$ corresponds to thermal ablation, while cld $= 1$ characterizes photophysical ablation which is related to the activated desorption of excited species.

Figue 6 shows the coldness cld as a function of intensity $\mathcal{I}_S \equiv I_S/I_b$ for different values of $\mathcal{A}_T$. For very small values of $\mathcal{A}_T$ the coldness increases with intensity. With $\mathcal{A}_T > 0.05$ it already saturates at values $\mathcal{I}_S \lessapprox 1$. With $\mathcal{A}_T > 0.1$ ($t_T = 10^{-9}$ s) and $\mathcal{I}_S > 1$ ($I_S = 10^7$ W/cm^2) ablation is photophysical with cld ≈ 1. Thus, even with nanosecond pulses, ablation may be mainly photophysical, depending on $\mathcal{A}_T$.

Subsequently, we discuss the spatial distribution of the temperature, the concentration of excited species, and the intensity. All quantities are normalized to the corresponding values at the surface $z = 0$.

The spatial distribution of the normalized temperature, $\Delta\tilde{\mathcal{T}}/\Delta\tilde{\mathcal{T}}_S \equiv \Delta\tilde{T}/\Delta\tilde{T}_S$ is shown in Fig. 7a for different values of $\mathcal{I}_S$ and $\mathcal{A}_T$. The width of the temperature distribution increases with intensity $\mathcal{I}_S$ and relaxation time $\mathcal{A}_T$. $\Delta\tilde{T}(z)/\Delta\tilde{T}_S$ is equal to unity with $z = 0$ and becomes zero for $z \to \infty$. On an expanded scale a maximum at some finite distance $z_0 \approx \mathcal{D}_T/\tilde{v} \ll 1$ can be seen (Fig. 7b, curve 1). This maximum is related to the (finite) optical penetration depth and the heat flux (7); it can cause an instability in the planar evaporation front [15]. Except near the surface with $z < 0.2$, the temperature distribution is independent of $\mathcal{D}_T$ if $\mathcal{D}_T \ll 1$. In the limiting case $\mathcal{D}_T = 0$ (19) yields

$$\Delta\tilde{\mathcal{T}}(z \gg \mathcal{D}_T/\tilde{v}) \approx \frac{1}{\tilde{v}}\tilde{\mathcal{T}}(z) - \tilde{\mathcal{N}}^*(z)\,. \tag{33}$$

Figure 7b (curve 2) shows the change in curvature for a ten times smaller absorption cross section σ.

The spatial distribution of $\tilde{\mathcal{N}}^*/\tilde{\mathcal{N}}_S^* \equiv \tilde{N}^*/\tilde{N}_S^*$ is plottet in Fig. 8 for different values of $\mathcal{I}_S$ and $\mathcal{A}_T$.

The spatial distribution of the intensity $\tilde{\mathcal{T}}/\mathcal{I}_S \equiv \tilde{I}/I_S$ is shown in Fig. 9 for different values of $\mathcal{I}_S$ and $\mathcal{A}_T$. Both $\tilde{\mathcal{N}}^*(z)$ and $\tilde{\mathcal{T}}(z)$ depend on the parameters $\mathcal{I}_S\mathcal{A}_T$ and $\tilde{v}/\mathcal{I}_S$. The dependence on the latter parameter is not very pronounced because $\tilde{v}/\mathcal{I}_S$ changes only slowly with $\mathcal{I}_S$ (this follows from Fig. 2a,b if we inspect the change in intersections $\Lambda_1 = \Lambda_2$). On the other hand $\tilde{\mathcal{N}}^*(z)$ and $\tilde{\mathcal{T}}(z)$ strongly change with the parameter $\mathcal{I}_S\mathcal{A}_T$. In fact, for constant $\tilde{v}$, this parameter determines the extension of the bleaching zone. The dash-dotted curves in Figs. 8 and 9 refer to the limiting case $\tilde{v} = 0$ and $\mathcal{I}_S\mathcal{A}_T = 5$ [see (28) and (29)]. The figures show that the extension of the bleaching zone strongly

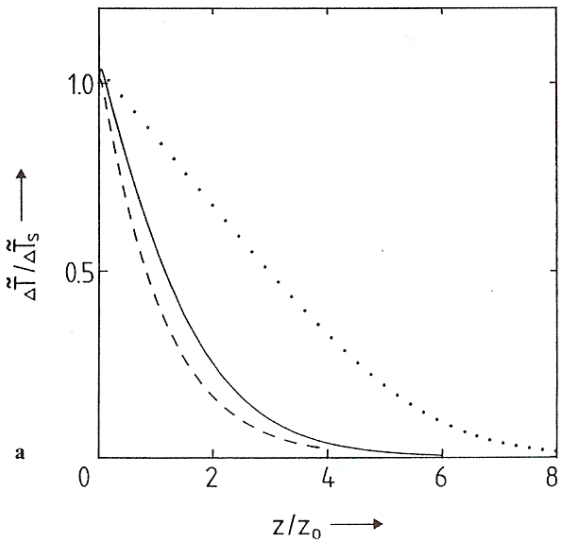

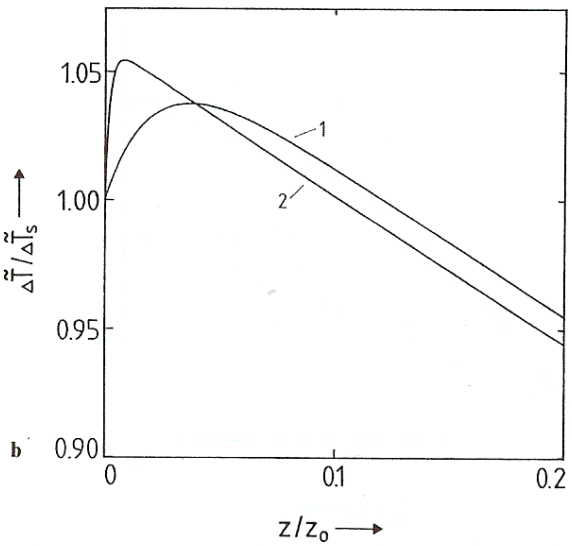

Fig. 7a–b. Spatial distribution of the stationary temperature, $\Delta\tilde{\mathcal{T}}(z)/\Delta\tilde{\mathcal{T}}_S \equiv \Delta\tilde{T}/\Delta\tilde{T}_S$ for $\mathcal{D}_T = 3.6 \times 10^{-2}$ and different parameters. **a** *Full curve*: $\mathcal{I}_S = 1$, $\mathcal{A}_T = 1$ ($\Delta\tilde{\mathcal{T}}_S = 0.28$); *dotted curve*: $\mathcal{I}_S = 5$, $\mathcal{A}_T = 1$ ($\Delta\tilde{\mathcal{T}}_S = 0.44$); *dashed curve*: $\mathcal{I}_S = 1$, $\mathcal{A}_T = 0.1$ ($\Delta\tilde{\mathcal{T}}_S = 0.62$). For all curves the cross section was $\sigma = 10^{-17}$ cm^2. **b** Curve 1: $\mathcal{I}_S = 1$, $\mathcal{A}_T = 1$, $\sigma = 10^{-17}$ cm^2; Curve 2: $\mathcal{I}_S = 1$, $\mathcal{A}_T = 1$, $\sigma = 10^{-18}$ cm^2

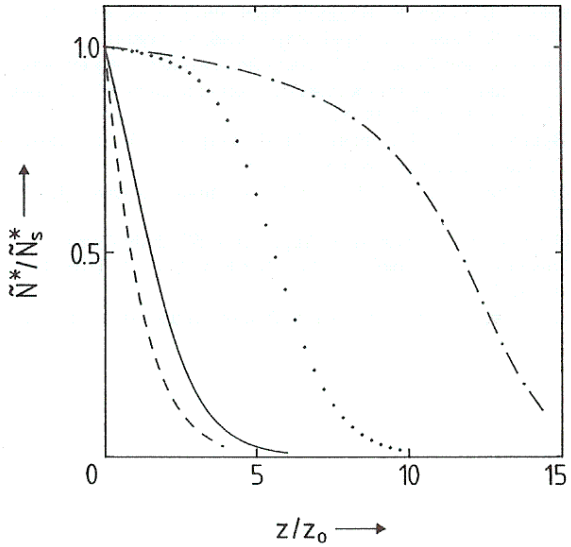

Fig. 8. Spatial distribution of the concentration of excited species $\tilde{\mathcal{N}}^*(\tilde{x})/\tilde{\mathcal{N}}_S^* \equiv \tilde{N}^*/\tilde{N}_S^*$ for different parameters. *Full curve*: $\mathcal{T}_S = 1$, $\mathcal{A}_T = 1$, $(\tilde{\mathcal{N}}_S^* = 0.29)$; *Dotted curve*: $\mathcal{T}_S = 5$, $\mathcal{A}_T = 1$ $(\tilde{\mathcal{N}}_S^* = 0.45)$; *Dashed curve*: $\mathcal{T}_S = 1$, $\mathcal{A}_T = 0.1$ $(\tilde{\mathcal{N}}_S^* = 0.008)$; *Dashed-dotted curve*: $\tilde{v} = 0$ $(\mathcal{T}_S\mathcal{A}_T = 5)$

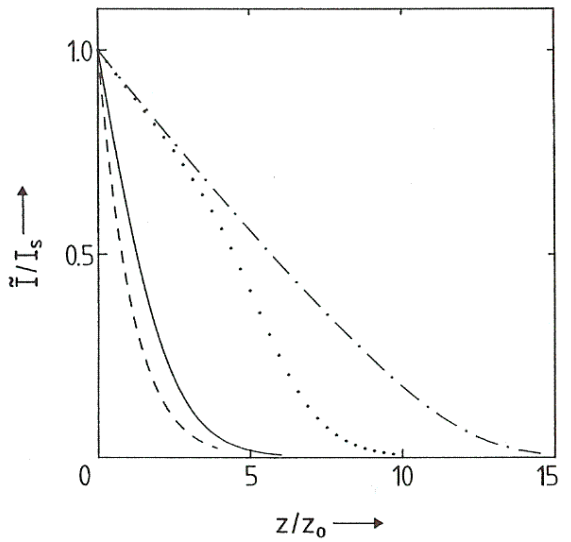

Fig. 9. Spatial distribution of laser-light intensity, $\tilde{\mathcal{I}}(\tilde{x})/\tilde{\mathcal{I}}_S \equiv \tilde{I}/I_S$ for different parameters. *Full curve*: $\mathcal{T}_S = 1$, $\mathcal{A}_T = 1$; *Dotted curve*: $\mathcal{T}_S = 5$, $\mathcal{A}_T = 1$; *Dashed curve*: $\mathcal{T}_S = 1$, $\mathcal{A}_T = 0.1$; *Dashed-dotted curve*: $\tilde{v} = 0$ $(\mathcal{T}_S\mathcal{A}_T = 5)$

decreases with ablation velocity $\tilde{v}$. This decrease is of the order $\Delta_{\tilde{x}} \approx \tilde{v}\mathcal{A}_T$. Thus, with the frequently made assumption $\tilde{v} = 0$, the width of the bleaching zone is significantly overestimated.

4 Summary and Conclusion

The model calculations described in this paper permit to interpret many features observed in UV-laser ablation of organic polymers. The main aspects, assumptions, and results of this model can be summarized as follows:

The total ablation velocity is determined by activated desorption of both ground-state species A and electronically excited species A^*; for the respective activation energies we assume $\Delta E \gg \Delta E^*$. The rate equations for species A and A^* are solved together with the heat equation. Here, the motion of the ablation front has been taken into consideration. The heat source term is controlled by thermal relaxation of the excitation energy which is described by a single time constant t_T. With activation energies of $\Delta E = 3$ eV to 5 eV, $\Delta E^* = 0.3$ eV and relaxation times $t_T > 10^{-9}$ s the model predicts realistic ablation rates at (moderate) surface temperatures of about 2000° C. This is an important difference to earlier calculations which predicted temperatures of (6–12) $\times 10^{3\circ}$ C near the ablation threshold [7]. If we assume a purely thermal process, i.e. if we set $t_T = 0$, the surface temperature obtained in our calculation rapidly increases with increasing ΔE. The value of $\Delta E = 3$ eV employed in the present calculations seems to be realistic for polyimide (dissociation energy of C–N bonds is about 3.15 eV [16]). In many cases, for example in aromatic compounds, the bond breaking energies exceed this value considerably ($\Delta E \approx 4.8$ eV for C–H and C–O bonds, and 4.5 eV for C–N bonds [13]). However, even with polyimide, the fragmentation and ablation process requires the breaking of several bonds, so that the effective activation energy may be higher even in this case. Anyway, with higher values of ΔE, the effects discussed in this paper are even more pronounced. The relaxation times employed seem to be realistic for some types of polymers, such as polyethyleneterephthalate and polyimide and photon energies higher than 4.4 eV, but below 6.2 eV. With photon energies higher than 6.2 eV, photochemical decomposition may dominate [9].

The present model ignores a number of effects which may be important for a quantitative description of the experimental data. Among those are non-stationary contributions to the ablation rate, the influence of stresses , multiple-photon excitations, etc. In the present form, the model cannot be applied to materials, where volume reactions become important as, e.g. in PMMA. It is evident that the description of the laser excitation and energy-dissipation processes on the basis of a two level system is a crude simplification. If we would consider a three-level or even more complex system, the relative contribution of single relaxation channels may change significantly. For example, with the laser-light intensities employed in polymer ablation, and with certain relaxation times, stimulated emission may become unimportant. Nevertheless, in spite of these simplifications, the model consistently describes many features observed in laser materials ablation.

Acknowledgements. We wish to thank Dr. R. Srinivasan for valuable comments on this paper and the "Fonds zur Förderung der wissenschaftlichen Forschung in Österreich" for financial support.

References

1. D.C. Paine, J.C. Bravman (eds.): *Laser Ablation for Materials Synthesis*. MRS Symp. Proc., Vol. 191 (MRS, Pittsburgh, PA 1990)
2. J.C. Miller, R.F. Haglund, Jr. (eds.): *Laser Ablation - Mechanisms and Applications*, Lect. Notes Phys., Vol. 389 (Springer, Berlin, Heidelberg 1991)

3. E. Fogarassy, S. Lazare (eds.): *Laser Ablation of Electronic Materials - Basic Mechanisms and Applications*, Proc. E-MRS, Vol. 4 (North-Holland, Amsterdam 1992)
4. R. Srinivasan, B. Braren: Chem. Rev. **89**, 1303 (1989)
   R. Srinivasan: In *Interfaces under Laser Irradiation*, NATO ASI Series, ed. by L.D. Laude, D. Bäuerle, M. Wautelet (Nijhoff, Dordrecht 1987) p. 359
5. D. Bäuerle, B. Luk'yanchuk, P. Schwab, X.Z. Wang, E. Arenholz: in Ref. [3] p. 39
6. S.R. Cain, F.C. Burns, C.E. Otis: J. Appl. Phys. **71**, 4107 (1992)
7. S.R. Cain, F.C. Burns, C.E. Otis, B. Braren: J. Appl. Phys. **72**, 5172 (1992)
8. R. Sauerbrey, G.H. Pettit: Appl. Phys. Lett. **55**, 421 (1989)
9. S. Küper, J. Brannon, K. Brannon: Appl. Phys. A **56**, 43 (1993)
10. G.H. Pettit, R. Sauerbrey: Appl. Phys. A **56**. 51 (1993)
11. J. Guillet: *Polymer Photophysics and Photochemistry*. An introduction to the study of photoprocesses in macromolecules. (Cambridge Univ. Press, Cambridge 1985)
12. Y.A. Bykovskii, V.N. Lisyutenko, M.M. Potapov, A.A. Chistyakov: Sov. J. Quant. Electron. **16**, 667 (1986)
13. G. Arjavalingam, G. Hougham, J.P. LaFemina: Polymer **31**, 840 (1990)
14. B.J. Garrison, R. Srinivasan: J. Appl. Phys. **57**, 2909 (1985)
15. S.I. Anisimov, M.I. Tribel'skii: Sov. Sci Rev: Sect. A; Phys. Rev. **8**, 259 (1987)
16. T.L. Cottrell: *Strength of Chemical Bonds* (Butterworths, London 1958)